

## Time-Resolved Measurements of Hot-Electron Equilibration Dynamics in High-Intensity Laser Interactions with Thin-Foil Solid Targets

P. M. Nilson,<sup>1,2</sup> J. R. Davies,<sup>1,2,3</sup> W. Theobald,<sup>2</sup> P. A. Jaanimagi,<sup>2</sup> C. Mileham,<sup>2</sup> R. K. Jungquist,<sup>2</sup> C. Stoeckl,<sup>2</sup> I. A. Begishev,<sup>2</sup> A. A. Solodov,<sup>1,2</sup> J. F. Myatt,<sup>2</sup> J. D. Zuegel,<sup>2</sup> T. C. Sangster,<sup>2</sup> R. Betti,<sup>1,2,3,4</sup> and D. D. Meyerhofer<sup>1,2,3,4</sup>

<sup>1</sup>Fusion Science Center for Extreme States of Matter, University of Rochester, Rochester, New York 14623, USA

<sup>2</sup>Laboratory for Laser Energetics, University of Rochester, Rochester, New York 14623, USA

<sup>3</sup>Department of Mechanical Engineering, University of Rochester, Rochester, New York 14623, USA

<sup>4</sup>Department of Physics, University of Rochester, Rochester, New York 14623, USA

(Received 7 October 2011; published 22 February 2012)

Time-resolved  $K_\alpha$  spectroscopy has been used to infer the hot-electron equilibration dynamics in high-intensity laser interactions with picosecond pulses and thin-foil solid targets. The measured  $K_\alpha$ -emission pulse width increases from  $\sim 3$  to 6 ps for laser intensities from  $\sim 10^{18}$  to  $10^{19}$  W/cm<sup>2</sup>. Collisional energy-transfer model calculations suggest that hot electrons with mean energies from  $\sim 0.8$  to 2 MeV are contained inside the target. The inferred mean hot-electron energies are broadly consistent with ponderomotive scaling over the relevant intensity range.

DOI: 10.1103/PhysRevLett.108.085002

PACS numbers: 52.50.Jm, 32.30.Rj, 52.38.Ph

High-intensity laser interactions with solid targets generate extreme states of matter [1] with unique energy-transport properties [2,3]. At laser intensities above  $10^{18}$  W/cm<sup>2</sup>, high-current electron beams with  $\sim$ MeV energies are generated [4–7], heating matter to high thermal temperatures over picosecond time scales [2,3,8]. Understanding the energy partition and its evolution in these highly nonequilibrium plasmas is an important open issue, underpinning applications in high-energy-density science [1], plasma-based particle acceleration [9], warm dense matter [10], high-peak-power  $\gamma$ -ray generation [11], and advanced inertial fusion energy concepts, including fast ignition [12]. In these conditions, the hot-electron equilibration dynamics are not completely understood, and accurate time-resolved measurements are required to test energy partition and temperature equilibration models.

The only previous hot-electron equilibration data in this regime are the time-resolved  $K_\alpha$ -emission data of Chen *et al.* [13]. Those experiments irradiated thin-foil targets with  $\sim 0.5$ -ps pulses focused to intensities up to  $10^{19}$  W/cm<sup>2</sup> and used the  $K_\alpha$ -emission pulse width to characterize the time scale for energy thermalization (“relaxation”) between hot and cold electrons. The data showed  $K_\alpha$ -emission pulse widths from  $\sim 12$  to 16 ps. The data were compared to an electron-energy-transfer model that included ion-front expansion and collisional electron-energy transfer based on Landau-Spitzer theory [14]. With increasing laser intensity, the model did not reproduce the rise time ( $\sim 10$  ps) or the duration of the measured  $K_\alpha$  signals, revealing an incomplete picture of the hot-electron equilibration dynamics.

In this Letter, ultrafast measurements of the hot-electron relaxation time in high-intensity laser-solid interactions are reported. Thin-foil targets were irradiated with 0.5- to 1-ps

pulses focused to intensities from  $\sim 10^{18}$  to  $10^{19}$  W/cm<sup>2</sup> and the hot-electron equilibration dynamics studied with time-resolved  $K_\alpha$  spectroscopy. In these interactions, the full width at half maximum (FWHM) of the  $K_\alpha$  signal increases with laser intensity from  $\sim 3$  to 6 ps. These are the first experiments at relativistic laser intensities to show rapid hot-electron relaxation times with  $K_\alpha$ -emission pulse widths up to a factor of  $4\times$  shorter than in previously reported experiments [13]. To provide insight into the mean energy of the hot electrons contained inside the target, the duration of the measured  $K_\alpha$  signals is compared to predictions from a collisional energy-transfer model. Assuming collisional energy transfer dominates, the data suggest that hot electrons with mean energies from  $\sim 0.8$  to 2 MeV are contained inside the target. The inferred mean hot-electron energies are broadly consistent with ponderomotive scaling [6] over the relevant intensity range.

The experiments were carried out with the Multi-Terawatt laser [15] at the University of Rochester’s Laboratory for Laser Energetics. Figure 1 shows a schematic of the experimental setup. The Multi-Terawatt laser delivered 1- to 10-J, 0.5- to 1-ps pulses at a wavelength of  $1.053\ \mu\text{m}$  that were focused by an  $f/3$  off-axis parabolic mirror to a spot with a FWHM of  $\sim 5\ \mu\text{m}$ , providing peak vacuum-focused intensities from  $\sim 10^{18}$  to  $10^{19}$  W/cm<sup>2</sup>. The laser-intensity contrast was  $\sim 10^8$  at 100 ps before the peak of the main laser pulse [16]. The laser was focused at normal incidence on  $500 \times 500 \times 20\text{-}\mu\text{m}^3$  Cu-foil targets mounted on  $17\text{-}\mu\text{m}$ -diameter silicon carbide stalks.

Time resolving the  $K_\alpha$  radiation generated in these experiments is a direct technique for inferring the hot-electron relaxation time [13].  $K_\alpha$  radiation emitted from the target was measured with a 2-ps time-resolution x-ray streak camera [17] coupled to a highly annealed pyrolytic graphite (HAPG) crystal spectrometer. The HAPG crystal

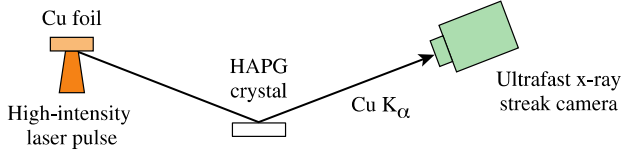


FIG. 1 (color online). Experimental setup. HAPG: highly annealed pyrolytic graphite.

was  $50 \times 14 \text{ mm}^2$  in area and had a three-dimensional, elliptically curved surface with radii  $R_1 = -22.000 \text{ mm}$  and  $R_2 = -10.620 \text{ mm}$  and conic constants  $k_1 = -0.825 \text{ mm}$  and  $k_2 = -0.955 \text{ mm}$ , collecting radiation from 7.8 to 8.5 keV. This spectral range covers the  $2p \rightarrow 1s$  transition in Cu, allowing for time-resolved Cu  $K_\alpha$  measurements at 8.05 keV.

The streak camera was independently characterized by direct illumination of the photocathode with a 10-mJ, 0.5-ps pulse of 263-nm light. Figure 2 shows a schematic of the setup. By passing half of the UV beam through a quartz plate of known thickness, two pulses were generated, providing a sweep-speed calibration. Figure 2(b) shows a typical streak-camera trace for these two pulses. The pulse widths (FWHM) are  $1.8 \pm 0.1$  and  $1.9 \pm 0.1$  ps. Temporal dispersion in the streak camera gives a slightly different impulse response for x-ray illumination. Monte Carlo modeling of the electron optics inside the streak tube shows that this offset is  $\sim 0.2$  ps, giving an impulse response for x rays of  $\sim 2$  ps.

Figure 3 shows an example of time-resolved plasma x-ray emission data for different high-intensity laser irradiation conditions. Figure 3(a) shows the time-resolved  $K_\alpha$  emission from a  $500 \times 500 \times 20\text{-}\mu\text{m}^3$  Cu foil irradiated with a 0.9-J, 0.6-ps pulse focused to  $3.6 \times 10^{18} \text{ W/cm}^2$ . The pulse width is  $3.0 \pm 0.2$  ps. Figure 3(b) shows the  $K_\alpha$  emission from a similar target irradiated with an 8.5-J, 0.8-ps pulse focused to  $2.9 \times 10^{19} \text{ W/cm}^2$ . The pulse width is  $5.5 \pm 0.1$  ps. The  $K_\alpha$  emission from these targets was measured as a peaked signal with a sharp rise and a slower decay. The signal rise time did not vary with laser intensity and was determined by the experimental resolution. The signal decay time increased with laser intensity and was sensitive to the hot-electron equilibration dynamics.

$K_\alpha$  radiation is generated in these experiments by hot electrons that are confined by target charging [7,18,19]. The thin-foil target rapidly charges because of the electrostatic potential that develops after the initial loss of a small fraction of high-energy electrons [18]. The remaining hot electrons ( $> 90\%$  of the total laser-accelerated population) make multiple round-trips of the target as they recirculate (reflux) because their collisional range is several hundred microns at solid density [20].

A collisional energy-loss model for understanding hot-electron relaxation and the time dependence of  $K_\alpha$  emission in these targets has been developed. The model

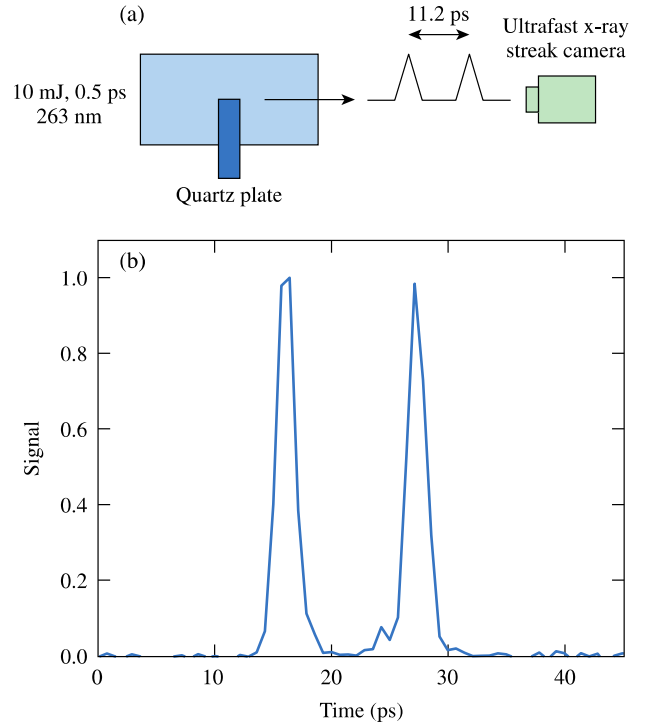


FIG. 2 (color online). (a) Streak-camera calibration setup. (b) Streak-camera response measurement with 0.5-ps, 263-nm pulses showing pulse widths of  $1.8 \pm 0.1$  and  $1.9 \pm 0.1$  ps.

calculates the  $K_\alpha$ -emission rate for a given hot-electron-energy distribution, assuming that all of the electrons are trapped inside the foil. The hot-electron-energy loss rate is given by [20]

$$\frac{dE}{dt} = -\frac{n_e e^4 L_d}{4\pi \epsilon_0^2 m_e v}, \quad (1)$$

where  $n_e$  is the electron density for solid Cu ( $2.46 \times 10^{24} \text{ cm}^{-3}$ ),  $E$  is the hot-electron energy,  $m_e$  is the electron rest mass,  $v$  is the hot-electron velocity,  $e$  is the electron charge, and  $\epsilon_0$  is the permittivity of free space. The stopping number  $L_d$  (or “ $\log \Lambda$ ”) depends weakly on material and the hot-electron energy, with values for Cu taken from Ref. [21]. The time spent by hot electrons outside the target during recirculation is assumed to be negligible, and energy losses to ion acceleration and self-generated electric fields are not considered in this model [7,18,19]. The implications for these assumptions on the inferred mean hot-electron energy will be discussed later.

$K_\alpha$ -emission pulse widths have been calculated for hot electrons with exponential ( $f_h \propto e^{-\gamma m_e c^2 / k_B T_h}$ ) and three-dimensional relativistic Maxwellian [ $f_h \propto \gamma(\gamma^2 - 1)^{1/2} e^{-\gamma m_e c^2 / k_B T_h}$ ] energy distributions, where  $f_h$  is the hot-electron-energy distribution function,  $k_B$  is Boltzmann’s constant,  $T_h$  is the hot-electron temperature, and  $\gamma$  is the Lorentz factor. Isochoric energy transfer to solid matter in these calculations is assumed. The

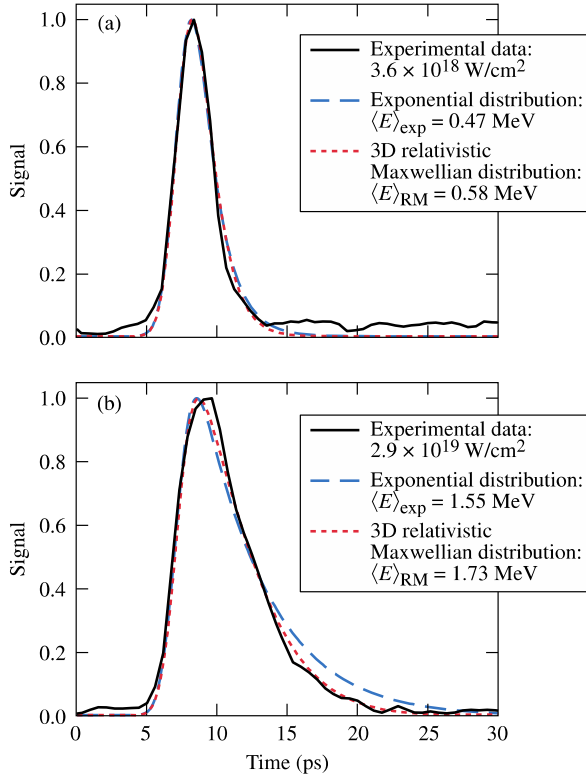


FIG. 3 (color online). Experimental time-resolved  $K_{\alpha}$ -emission data from  $500 \times 500 \times 20\text{-}\mu\text{m}^3$  Cu foils. The targets were irradiated with (a) a 0.9-J, 0.6-ps pulse and (b) an 8.7-J, 0.8-ps pulse. The data are shown with theoretical fits based on a collisional energy-loss model with exponential (long-dashed line) and 3D relativistic Maxwellian (short-dashed line) hot-electron-energy distributions.

$K_{\alpha}$ -emission rate is proportional to the Cu-ion density, the time-varying number of hot electrons, and the parameter  $\langle \sigma_K v \rangle$  averaged over the hot-electron-energy distribution, where  $\sigma_K$  is the  $K$ -shell ionization cross section and  $v$  is the hot-electron velocity. On the time scale of the detection, the conversion of hot-electron energy to a  $K_{\alpha}$  photon is considered to be instantaneous. The cross section for ionization of  $K$ -shell electrons was taken from Ref. [21].

Figure 3 shows synthetic  $K_{\alpha}$  streaks that were calculated from this model. The synthetic pulse widths were fit to the data by adjusting the signal intensity and the mean hot-electron energy in the model. They represent a convolution of the calculated  $K_{\alpha}$ -emission rate with the laser-pulse duration and the temporal resolution of the x-ray streak camera. In the low-intensity case [Fig. 3(a)], the model predicts well the  $K_{\alpha}$ -emission pulse shape, independent of the hot-electron-energy distribution that was used. The best fit of the experimental data was obtained with the parameters  $\langle E \rangle_{\text{exp}} = 0.47 \text{ MeV}$  for the exponential energy distribution and  $\langle E \rangle_{\text{RM}} = 0.58 \text{ MeV}$  for the 3D relativistic Maxwellian energy distribution. In the high-intensity case [Fig. 3(b)], the best fit was obtained with the

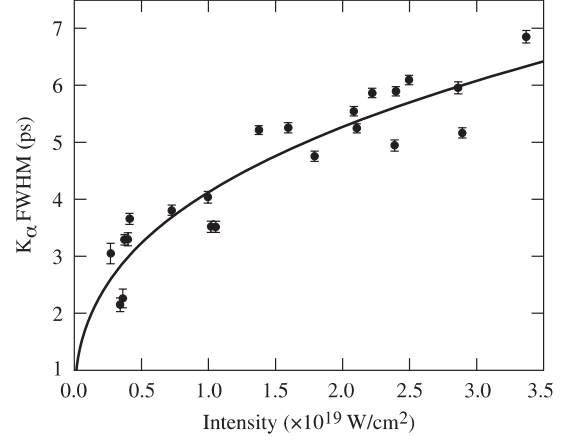


FIG. 4. Experimental  $K_{\alpha}$ -emission pulse width as a function of laser intensity. The pulse widths have been adjusted to account for the impulse response of the streak camera.

parameters  $\langle E \rangle_{\text{exp}} = 1.55 \text{ MeV}$  and  $\langle E \rangle_{\text{RM}} = 1.73 \text{ MeV}$ . In this case, the  $K_{\alpha}$ -emission pulse shape was better reproduced by model calculations with a 3D relativistic Maxwellian energy distribution.

Figure 4 shows the variation with increasing laser intensity of the measured  $K_{\alpha}$ -emission pulse width. An upper estimate of the true  $K_{\alpha}$ -emission pulse width was obtained by accounting for instrumental effects, subtracting the FWHM of the impulse response function from the streak-camera trace in quadrature. Gaussian pulse shapes are assumed. For laser intensities between  $2.7 \times 10^{18}$  and  $3.4 \times 10^{19} \text{ W/cm}^2$ , the duration of the measured  $K_{\alpha}$  signal increases from  $\sim 3$  to 6 ps. Over this intensity range, a least-squares fit shows that the  $K_{\alpha}$ -emission pulse width increases with laser intensity and is given by  $\tau_{K_{\alpha}}[\text{ps}] = (4.1 \pm 0.3)I_{19}^{0.35 \pm 0.07}$ , where  $I_{19}$  is the laser intensity in units of  $10^{19} \text{ W/cm}^2$ .

To obtain a mean hot-electron-energy scaling, these data were compared with the collisional energy-loss model. Figure 5(a) shows the relationship between the calculated  $K_{\alpha}$ -emission pulse width and the mean hot-electron energy for exponential and 3D relativistic Maxwellian energy distributions. In these calculations, the  $K_{\alpha}$ -emission rate was convolved with a 0.8-ps FWHM Gaussian pulse that approximated the range of laser-pulse durations that were used in these experiments. The synthetic pulse was convolved with a 2-ps FWHM Gaussian instrument response that was removed in quadrature for comparison with the experimental data (Fig. 4). Figure 5(a) shows that calculations with a 3D relativistic Maxwellian energy distribution have slightly higher mean hot-electron energies than with an exponential energy distribution for a given  $K_{\alpha}$ -emission pulse width. This offset is  $\sim 100$  to 200 keV.

Figure 5(b) shows the mean hot-electron energies that are inferred from the experimental data based on this model. Two scaling laws are obtained: For an exponential energy distribution,  $\langle E \rangle_{\text{exp}}[\text{MeV}] = (1.12 \pm 0.11)I_{19}^{0.51 \pm 0.11}$ .

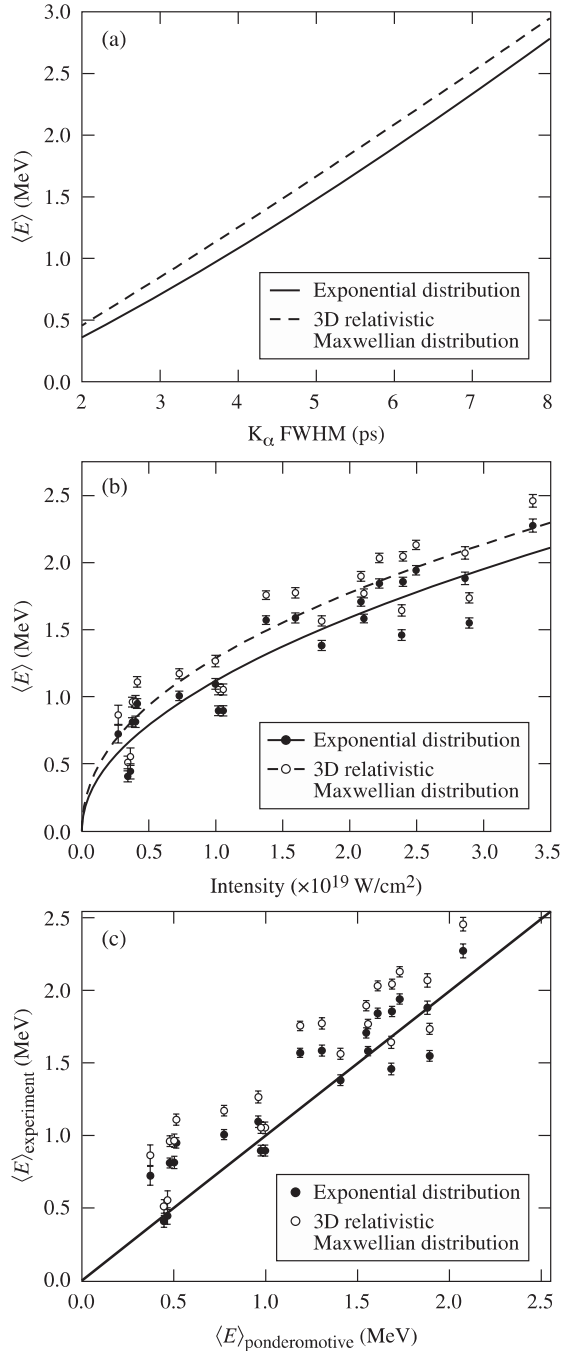


FIG. 5. (a) Calculated mean hot-electron energy  $\langle E \rangle$  as a function of  $K_\alpha$ -emission pulse width based on a 0.8-ps laser-pulse duration. (b) Inferred  $\langle E \rangle$  as a function of laser intensity, assuming exponential (solid line) and 3D relativistic Maxwellian (dashed line) hot-electron-energy distributions. (c) Comparison of the experimentally inferred  $\langle E \rangle$  with ponderomotive scaling [6].

For a 3D relativistic Maxwellian energy distribution,  $\langle E \rangle_{\text{RM}}[\text{MeV}] = (1.19 \pm 0.11)I_{19}^{0.46 \pm 0.10}$ . Assuming collisional energy transfer dominates, these results show that mean hot-electron energies from  $\sim 0.8$  to 2 MeV are required to generate  $K_\alpha$ -emission pulse widths consistent with the experimental observations.

Figure 5(c) compares these inferred mean hot-electron energies with ponderomotive scaling [6]. Ponderomotive scaling gives  $\langle E \rangle = m_e c^2 [1 + (2U_p/m_e c^2)]^{1/2}$ , where  $U_p = 9.33 \times 10^{-14} I[\text{W/cm}^2](\lambda[\mu\text{m}])^2$  is the ponderomotive potential. In each case, the inferred mean energies are slightly higher compared with ponderomotive scaling. The best agreement was found for calculations with an exponential energy distribution. A similar scaling predicting  $\sim 100$  to 200 keV higher mean hot-electron energies was found with calculations using the 3D relativistic Maxwellian energy distribution. Compared with ponderomotive scaling, the power law fits give a faster increase in mean energy with intensity near  $10^{18}$  W/cm $^2$  and provide a better fit to the experimental data.

The collisional energy-loss model presented here is not intended to fully model the experiment but is used to help interpret the data. The model neglects energy loss to self-generated electric fields and to ion acceleration, and it neglects the time electrons take to be reflected by the electrostatic field outside the target. All of these effects would be expected to increase with laser intensity, and an accurate assessment of them will require numerical modeling. The accuracy with which the collisional model reproduces all of the experimental results and the relative insensitivity of the mean energy to the energy distribution indicates that the values are likely not significantly in error. Measurements of the ion emission at these intensities show that it is not a significant energy sink [22]. The results presented here form a comprehensive test bed for future comparison with numerical modeling that may include these effects.

In summary, the hot-electron equilibration dynamics in thin-foil solid targets irradiated with high-intensity laser pulses have been studied. Time-resolved  $K_\alpha$  spectroscopy measurements show  $K_\alpha$ -emission pulse widths from  $\sim 3$  to 6 ps for laser intensities between  $\sim 10^{18}$  and  $10^{19}$  W/cm $^2$ . Assuming collisional energy transfer dominates, the experimental data suggest that hot electrons with mean energies from  $\sim 0.8$  to 2 MeV are contained inside the target. The inferred mean hot-electron-energy scaling with laser intensity is broadly consistent with ponderomotive scaling. These findings are important for the understanding of a wide range of high-energy-density physics applications that require a large and fast energy input into matter.

This work was supported by the U.S. Department of Energy Office of Inertial Confinement Fusion under Cooperative Agreement No. DE-FC52-08NA28302, the University of Rochester, and the New York State Energy Research and Development Authority.

- [1] B. A. Remington *et al.*, *Science* **284**, 1488 (1999).
- [2] J. A. Koch *et al.*, *Phys. Rev. E* **65**, 016410 (2001); K. Eidmann *et al.*, *J. Quant. Spectrosc. Radiat. Transfer* **81**,

- 133 (2003); P. Audebert *et al.*, *Phys. Rev. Lett.* **94**, 025004 (2005).
- [3] C. R. D. Brown *et al.*, *Phys. Rev. Lett.* **106**, 185003 (2011).
- [4] D. F. Price *et al.*, *Phys. Rev. Lett.* **75**, 252 (1995); H. Chen *et al.*, *Phys. Rev. Lett.* **70**, 3431 (1993); K. B. Wharton *et al.*, *Phys. Rev. Lett.* **81**, 822 (1998); K. Yasuike *et al.*, *Rev. Sci. Instrum.* **72**, 1236 (2001); S. P. Hatchett *et al.*, *Phys. Plasmas* **7**, 2076 (2000).
- [5] F. N. Beg *et al.*, *Phys. Plasmas* **4**, 447 (1997).
- [6] S. C. Wilks *et al.*, *Phys. Rev. Lett.* **69**, 1383 (1992).
- [7] P. M. Nilson *et al.*, *Phys. Rev. Lett.* **105**, 235001 (2010); *Phys. Plasmas* **18**, 056703 (2011).
- [8] A. Saemann *et al.*, *Phys. Rev. Lett.* **82**, 4843 (1999); P. Audebert *et al.*, *Phys. Rev. Lett.* **89**, 265001 (2002).
- [9] E. L. Clark *et al.*, *Phys. Rev. Lett.* **84**, 670 (2000); R. A. Snavely *et al.*, *Phys. Rev. Lett.* **85**, 2945 (2000).
- [10] P. K. Patel *et al.*, *Phys. Rev. Lett.* **91**, 125004 (2003).
- [11] P. A. Norreys *et al.*, *Phys. Plasmas* **6**, 2150 (1999).
- [12] M. H. Key *et al.*, *Phys. Plasmas* **5**, 1966 (1998); M. Tabak *et al.*, *Phys. Plasmas* **1**, 1626 (1994).
- [13] H. Chen *et al.*, *Phys. Rev. E* **76**, 056402 (2007).
- [14] L. D. Landau, *Phys. Z. Sowjetunion* **10**, 154 (1936); L. Spitzer, *Physics of Fully Ionized Gases*, Interscience Tracts on Physics and Astronomy (Wiley Interscience, New York, 1962), 2nd revised ed.
- [15] V. Bagnoud *et al.*, *Opt. Lett.* **30**, 1843 (2005).
- [16] V. Bagnoud *et al.*, *Opt. Express* **15**, 5504 (2007).
- [17] C. Stoeckl *et al.*, *Bull. Am. Phys. Soc.* **52**, 67 (2007).
- [18] J. Myatt *et al.*, *Phys. Plasmas* **14**, 056301 (2007).
- [19] A. J. Mackinnon *et al.*, *Phys. Rev. Lett.* **88**, 215006 (2002); Y. Sentoku *et al.*, *Phys. Plasmas* **10**, 2009 (2003); W. Theobald *et al.*, *Phys. Plasmas* **13**, 043102 (2006); S. D. Baton *et al.*, *High Energy Density Phys.* **3**, 358 (2007); P. M. Nilson *et al.*, *Phys. Plasmas* **15**, 056308 (2008); *Phys. Rev. E* **79**, 016406 (2009).
- [20] H. O. Wyckoff, *ICRU Report* (International Commission on Radiation Units and Measurements, Inc., Bethesda, MD, 1984).
- [21] J. P. Santos, F. Parente, and Y.-K. Kim, *J. Phys. B* **36**, 4211 (2003); <http://physics.nist.gov/PhysRefData/Star/Text/ESTAR.html>.
- [22] L. Robson, P. T. Simpson, R. J. Clarke, K. W. D. Ledingham, F. Lindau, O. Lundh, T. McCanny, P. Mora, D. Neely, C.-G. Wahlström, M. Zepf, and P. McKenna, *Nature Phys.* **3**, 58 (2006); J. Fuchs, P. Antici, E. D'Humières, E. Lefebvre, M. Borchesi, E. Brambrink, C. A. Cacchetti, M. Kaluza, V. Malka, M. Manclossi, S. Meyroneinc, P. Mora, J. Schreiber, T. Toncian, H. Pépin, and P. Audebert, *Nature Phys.* **2**, 48 (2005).